Aeroelastic analysis of a very large wind turbine in various atmospheric stability conditions

Dangi, Nirav; Yu, Wei; Sodja, Jurij; Ferreira, Carlos Simão

DOI
10.1088/1742-6596/2767/5/052026

Publication date
2024

Document Version
Final published version

Published in
Journal of Physics: Conference Series

Aeroelastic analysis of a very large wind turbine in various atmospheric stability conditions

Journal of Physics: Conference Series **2767** (2024) 052026 doi:10.1088/1742-6596/2767/5/052026

Aeroelastic analysis of a very large wind turbine in various atmospheric stability conditions

Nirav Dangi, Wei Yu, Jurij Sodja and Carlos Simão Ferreira

Aerospace Engineering, Delft University of Technology, 2629 HS Delft, The Netherlands

E-mail: n.s.dangi@tudelft.nl

Abstract. With the growing trend towards larger wind turbine rotor diameters, the impact of wind shear on rotor performance and loads becomes increasingly significant. Atmospheric stability strongly influences wind shear, leading to higher wind shear under stable atmospheric conditions. In this study, the aeroelastic performance of the IEA 22 MW rotor is assessed under inflow conditions generated by different methods. Inflow conditions were generated using turbulence models specified in the IEC Standards and also by Large Eddy simulations. Standalone OpenFAST simulations were conducted with the respective inflow conditions.

It was found that at rated and above-rated wind speeds, the time-averaged wind turbine design loads were higher in stable atmospheric conditions, in comparison to the IEC NTM inflow conditions, while the opposite held for below-rated wind speeds. Specifically, the time-averaged root flapwise bending moment and rotor thrust were found to be higher by up to 7% in stable atmospheres. However, maximum design and fatigue loads were considerably higher in the IEC NTM case due to elevated turbulence levels. Compared to the IEC NTM case, the damage equivalent root flapwise bending moment was found to be 30% to 70% lower in the different scenarios.

1. Introduction

Atmospheric stability strongly influences wind shear, with higher wind shear under stable atmospheric conditions ([1, 2]). The existing IEC standards ([3]) and design load cases for wind turbine fatigue analysis do not explicitly incorporate atmospheric stability. Consequently, using more realistic wind fields in load calculations may lead to design loads differing from those prescribed by the IEC standards, especially, when designing larger rotors. With the upcoming 20 MW and above wind turbines, the rotor diameter extends well above 250 m ([4, 5]). It thus becomes necessary to carefully assess the performance of wind turbine rotors in conditions where the rotor extends well beyond the atmospheric surface layer and is exposed to, for instance, different turbulence intensities and wind shear through the span ([6]).

Existing literature assessing the impact of atmospheric stability on wind turbine rotor loads can be found in ([7, 8, 9, 10, 11]). However, most studies are conducted on comparatively smaller wind turbines, with lower hub heights and rotor diameters. The study of [8] is on a 2 MW wind turbine with 70 m hub height. The authors of [9] conduct a study on the NREL 5 MW reference wind turbine with a hub height of 90 m. In [10], the study is conducted on a 5.5 MW reference wind turbine with a hub height of 95 m. Larger rotors are associated with higher flexibility and more complex aeroelastic effects and, thus, need further investigation under such varied atmospheric conditions. Furthermore, most studies use analytical formulations rather than

higher-fidelity methods to generate atmospheric boundary layer inflows. One research paper that incorporated a more powerful wind turbine and a higher fidelity inflow is [11], conducted for the AVATAR 10 MW wind turbine with a hub height of 132.7 m. Among other recommendations, the authors of [11] recommend to have future studies focus on larger tower heights and assess the turbulence characteristics at larger heights.

The current study contributes to the state of the art by assesing the IEA 22 MW RWT (research wind turbine) [4, 12] with a hub height of 170 m under various inflow conditions , in comparison to the IEC guidelines. Three different atmospheric stability conditions are considered for three different wind speeds. Furthermore, the fatigue expectations in such conditions are studied to determine whether the trends are similar to existing studies on smaller wind turbines, and whether the IEC guidelines lead to conservative results. The theory behind the different inflow conditions is provided in section 2, followed by section 3, which explains the simulation set up. The results are discussed in section 4, and concluding remarks are placed in section 5.

2. Inflow Profile Generation

The simulations in this study were conducted with inflow conditions generated by means of a lower fidelity and a higher fidelity method. The lower fidelity method involved the use of TurbSim [13]. The higher fidelity method, on the other hand, utilised NREL SOWFA [14] coupled with CFD code OpenFOAM [15].

TurbSim is a stochastic, full-field, turbulence simulator which provides a numerical simulation of a full-field flow. It uses a statistical model, as opposed to a physics-based model to numerically simulate time series of three-component wind-speed vectors at points in a two-dimensional vertical rectangular grid that is fixed in space. TurbSim output can be used as input into InflowWind-based aeroelastic tools such as OpenFAST. InflowWind uses Taylor's frozen turbulence hypothesis to obtain local wind speeds, interpolating the TurbSim-generated fields in both time and space.

SOWFA is a high fidelity tool which is a set of computational fluid dynamics (CFD) solvers, boundary conditions, and turbine models. SOWFA simulates the atmospheric boundary layer (ABL) . ABL is the bottom 0.3 km to 3 km of the troposphere and is often turbulent, and varies in thickness in space and time. The conditions in atmospheric boundary layer are determined by the effects of the Earth's surface, which slows the wind due to surface drag, warms the air during daytime and cools it at night, and changes in moisture and pollutant concentration [1]. SOWFA is a solver governed by large-eddy simulation (LES) filtered continuity, momentum and potential temperature equations [16]. The momentum equation includes the buoyant forces using the Boussinesq approximation, without the need to recast the governing incompressible Navier-Stokes equations equations in a compressible form. It also incorporates the Coriolis force due to planetary rotation, a uniform pressure gradient driving the flow and subfilter scale (SFS) momentum fluxes. The solver employs a wall model for surface stresses close to the ground, in accordance with Monin-Obukhov similarity theory. The solver is used in a domain without the wind turbines and is called a precursor simulation [17]. The boundary conditions can be set such that the flow is cycling repeatedly through the domain. A pressure gradient can be applied to control the mean velocity and direction of the flow at a specific height to a predefined value. At the ground surface, a roughness value can be set and a predefined temperature flux can be used to generate diabatic wind fields. The simulation starts with an initial uniform velocity, pressure, and temperature field and as the simulation progresses, a certain shear profile and turbulence develops.

3. Simulation Set-up

The wind turbine under study was the v0.0.1 IEA 22 MW research wind turbine (RWT) [4, 12]. A brief overview of the turbine parameters and operational conditions are provided in Table 1.

Table 1: IEA 22 MW RWT specifications [4, 12]

Parameter	**Value**
Rated power	22 MW
Rated wind speed	10.94 m/s
Hub height	170 m
Rotor diameter	283.2181 m
Rated tip speed ratio	≈ 9

The objectives of this study were realised by assessing the wind turbine aerodynamic and structural performance by using NREL OpenFAST [18]. The generation of wind fields with the lower fidelity method, can be done by a variety of turbulence models are available in TurbSim. The IEC Kaimal turbulence model was used for the purpose of this study, with the IEC normal turbulence model (NTM), B type. The inflow conditions were generated for 660 s with a timestep of 0.05 s. In the higher fidelity method, a timestep of around 0.5 s, varying according to a maximum Courant number of 0.75 was chosen to restrict computational expense. The turbulence was assumed to reach a quasi-steady state after 20000 s, such a value has also been chosen in previous studies [17, 19]. The quasi-steady state was further checked by assessing planar average statistics and shear profile development in the stream-wise direction. The next 660 s of the wind field were used as inflow conditions to the standalone OpenFAST simulations. The important simulation inputs are specified in Table 2.

For both the methods, three different wind speed conditions were chosen, which were, below, around and above the rated wind speed of the IEA 22 MW wind turbine. The values were roughly 8.5 m/s, 11.5 m/s, and 14.5 m/s, respectively, at the hub height respectively. In the higher fidelity method, three different cases were chosen as stable (SABL), neutral (NABL) and unstable (USABL) atmospheric conditions. In the lower fidelity method, two different cases were chosen: inflow conditions corresponding to IEC NTM specifications, and a IEC NTM scaled turbulence intensity (TI) scenario. The scaling was done by scaling the standard deviation of the wind components at hub height to the standard deviations obtained by the higher fidelity method. The scaled IEC NTM scenario was chosen, for one, to allow for result discrepancies mainly by the wind profile rather than also by turbulence intensity. Secondly, it was chosen because the IEC NTM-B model yields a turbulence intensity of about 17% for a hub height wind speed of 11.5 m/s, while for the high fidelity method the hub height turbulence intensity was less than 5%, as will be explained later.

Table 2: Higher fidelity inflow conditions parameters. These values hold for the 3 different wind speed cases under investigation.

Scenario	**Surface roughness (m)**	**Temperature flux** (Km/s)	$L_x \times L_y \times L_z$	$N_x \times N_y \times N_z$
Stable atmosphere (SABL)		+0.02 in altitude direction		
Neutral atmosphere (NABL)	0.0001	0	3000×3000×1000	300×300×100
Unstable atmosphere (USABL)		−0.02 in altitude direction		

As listed in Table 2, the surface temperature flux was specified to generate either the stable or the unstable atmosphere. The choice of surface roughness, $z_0 = 0.0001$ m, characteristic of offshore conditions, was based on approximation by numerically solving the implicit Charnock's relation as shown below:

$$z_0 = \frac{A_c}{g}\left[\frac{\kappa V_{hub}}{ln\frac{z_{hub}}{z_0}}\right]^2 \tag{1}$$

In the above equation, A_c is Charnock's constant and is recommended to be 0.011 for open sea [3], $\kappa = 0.4$ is von Karman's constant, $g = 9.81$ m/s^2 is acceleration due to gravity and $z_{hub} = 170$ m is the hub height of the IEA 22 MW wind turbine. Upon using a hub height velocity of 11.5 m/s,

numerically solving the above equation yields $z_0 = 0.00011\,\text{m}$. The input surface roughness was set the same for all the simulations and not varied with velocity at hub height. Primarily because it has been noted that the effect of surface roughness on the average turbulence level is limited [19]. The Coriolis parameter was calculated using a latitude of 52.8 deg, representative of the Dutch North sea [20]. A capping inversion at 500 m was set for all simulations. The reference potential temperature was set as 300K. The reference wind speed was set as the corresponding value for the different cases, at hub height.

The simulations were run using DelftBlue, the TU Delft supercomputer [21]. Each simulation domain had 9 million cells and each simulation was run using 32 cores on 1 node, and had a wall clock time of around 72 hours.

For the wind turbine performance analysis in OpenFAST, the simulations were conducted for 660 s with a time step of 5 ms. As this time step is significantly lower than the time step of the inflow wind field, a quadratic interpolation was specified in the OpenFAST file. The first 60 s of the simulations were considered as an initial transient and were excluded from result analysis. The calculation of structural dynamics was done using the ElastoDyn module which uses the Euler-Bernoulli beam theory and does not have blade- torsion degree of freedom. The aerodynamic loads were calculated using the AeroDyn module with the blade element momentum theory and the Beddoes-Leishman dynamic stall model. The ServoDyn module with the NREL ROSCO controller [22] was used for the wind turbine control. In the ElastoDyn module, the degrees of freedom of the wind turbine blade and generator were enabled while the tower was assumed as rigid. In the AeroDyn module, the tower influence on the wind field was disabled to use the inflow as generated by the respective methods.

3.1. Input wind conditions

In this section the wind field used as inflow conditions is presented and discussed. The time-averaged values of the horizontal wind speed are shown below; calculated as $\sqrt{\overline{U}^2 + \overline{V}^2}$, where U and V are the X (stream-wise) and Y (lateral) component of velocity, respectively.

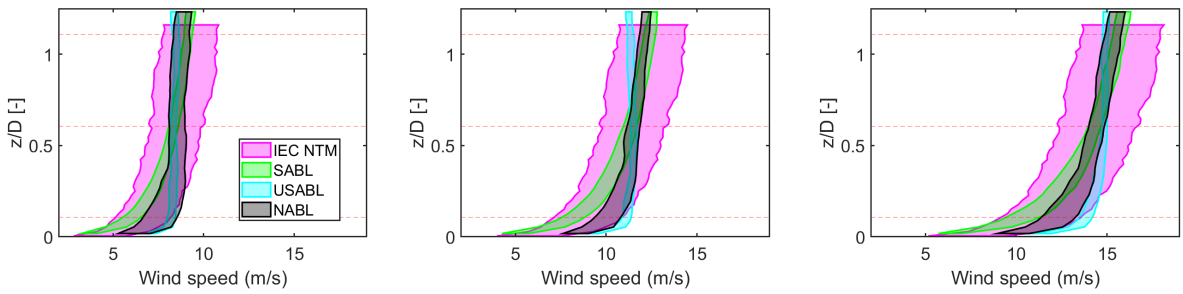

Figure 1: Time-averaged inflow profile. The patches indicate 1 times the standard deviation of the U component, on each side. The red lines indicate the top- tip, hub and bottom- tip heights. a) Below rated ($V_{hub} = 8.5\,\text{m/s}$) b) Around Rated ($V_{hub} = 11.5\,\text{m/s}$) c) Above rated ($V_{hub} = 14.5\,\text{m/s}$)

In Figure 1, the wind speed profile across different altitudes is shown for various wind speed and stability scenarios. The IEC NTM profile essentially represents a wind speed profile with a power-law exponent of 0.14 [3]. The other profiles represent the time-averaged profiles obtained under different atmospheric stability conditions. It can be noted that an unstable atmosphere leads to a wind profile that varies less with altitude, while increasing shear is observed in the

wind speed profiles in neutral and stable atmospheric conditions. Next, it was found that the hub height turbulence intensity was around 3% to 4% for all the cases, owing to the the high hub height of 170 m (Table 1) and a very low surface roughness of $z_0 = 0.0001$ m (Table 2). This magnitude of low turbulence intensity at such altitude is also evident in the results provided in Figure 5 of [11]. The IEC NTM-B model which uses the relation $\sigma = I_{ref}(0.75\mathrm{V_{hub}} + b)$, where $b = 5.6$ m/s, and $I_{ref} = 0.14$, leads to a considerably higher standard deviation as visible in Figure 1.

Lastly, to quantify the wind shear, an estimate of the wind shear exponent (α) for the different wind profiles is provided in Table 3. This is based on the wind profile power law as $\frac{V}{V_{ref}} = (\frac{z}{z_{ref}})^{\alpha}$. Here, the reference velocity V_{ref} and the reference height z_{ref} was chosen as the velocity at the hub height and the hub height respectively.

Table 3: Wind shear exponent comparison

Scenario	Below rated ($V_{hub} = 8.5$ m/s)	Around Rated ($V_{hub} = 11.5$ m/s)	Above rated ($V_{hub} = 14.5$ m/s)
Stable atmosphere	0.18	0.18	0.18
Neutral atmosphere	0.07	0.08	0.10
Unstable atmosphere	0.03	0.03	0.04
IEC offshore guideline		0.14	

The estimates in Table 3 are provided using non linear least square fitting to the wind profile power law equation, using the Levenberg-Marquardt algorithm in MATLAB [23]. It is evident that the stable atmosphere has the highest wind shear, while the unstable atmosphere has the lowest wind shear. It should be noted that the wind shear could be different in various other atmospheric conditions based on the surface flux and other parameters specified in the Large eddy simulations, investigating which is the focus of future studies.

4. Results and Discussion

In this section, the results of the wind turbine's aerodynamic and structural performance under various inflow conditions are presented. First, the normal force (perpendicular to chord line) variation along the different inflow conditions is shown in Figure 2.

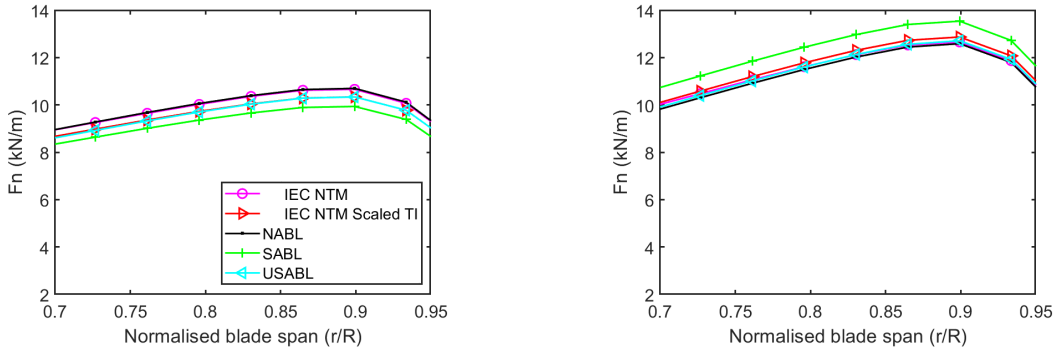

Figure 2: Normal force (to chord): Time-averaged plots (a,b,c). a) Below rated ($V_{hub} = 8.5$ m/s) b) Around Rated ($V_{hub} = 11.5$ m/s) c) Above rated ($V_{hub} = 14.5$ m/s) d) Maximum values at 0.85 r/R at different wind speeds. Figure continues on next page.

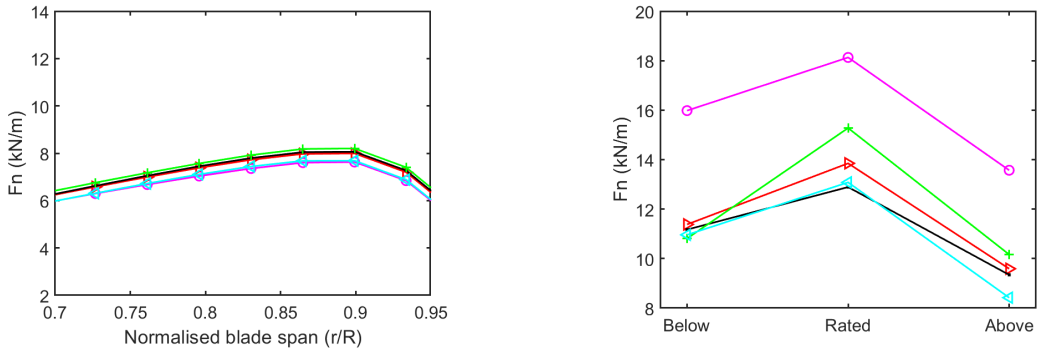

(c) (d)

Figure 2: Normal force (to chord): Time-averaged plots (a,b,c). a) Below rated ($V_{hub} = 8.5\,\mathrm{m/s}$) b) Around Rated ($V_{hub} = 11.5\,\mathrm{m/s}$) c) Above rated ($V_{hub} = 14.5\,\mathrm{m/s}$) d) Maximum values at 0.85 r/R at different wind speeds

In Figure 2, it can be observed that the normal force trend depends on the inflow conditions in general and the point of operation of the wind turbine. Below rated wind speeds, that is, in Figure 2a, the time-averaged normal force is lowest for the SABL inflow. The axial induction factor in this scenario was found to be the highest for the IEC NTM conditions while lower for the other inflow conditions. The power output in the NABL inflow was found to be the highest.

For the rated and above rated operation of the wind turbine, it can be noted that the time-averaged normal force is higher for the SABL inflow while lower for the IEC NTM conditions. Notably, the IEC NTM Scaled TI scenario also has a lower normal force than the SABL profile, suggesting that the change in normal force is dominated by the wind shear (Table 3) Around the rated operation, the time-averaged angle of attack was found to be higher by upto 1 deg for the SABL case, in comparison to the IEC NTM case. The time-averaged normal force was found to be higher by upto 7% in the SABL scenario, in comparison to the IEC NTM scenario. However, it can be seen in Figure 2d that the maximum normal force is lower by upto 38% for the different scenarios, in comparison to the IEC NTM scenario, which is a representative design driver, instead of the time-averaged normal force. Next, Figure 3 indicates the trend of the flapwise deflection along the blade tip region for the different inflow conditions.

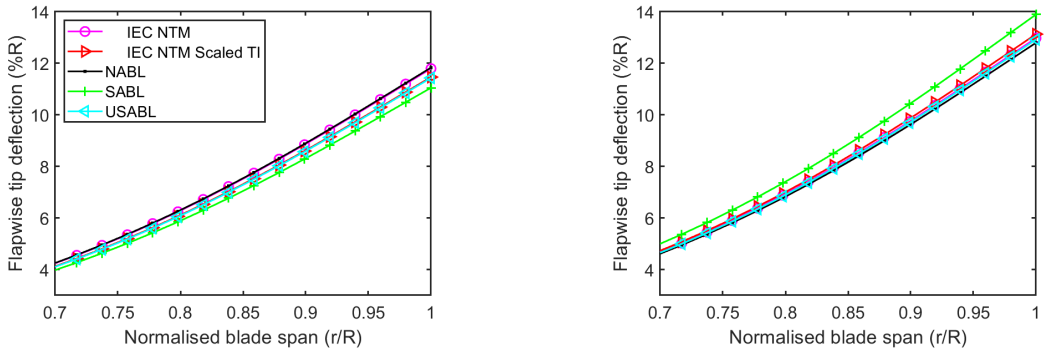

(a) (b)

Figure 3: Normalised blade tip flapwise displacement: Time-averaged plots (a,b,c). a) Below rated ($V_{hub} = 8.5\,\mathrm{m/s}$) b) Around Rated ($V_{hub} = 11.5\,\mathrm{m/s}$) c) Above rated ($V_{hub} = 14.5\,\mathrm{m/s}$) d) Maximum values at tip, at different wind speeds. Figure continues on next page.

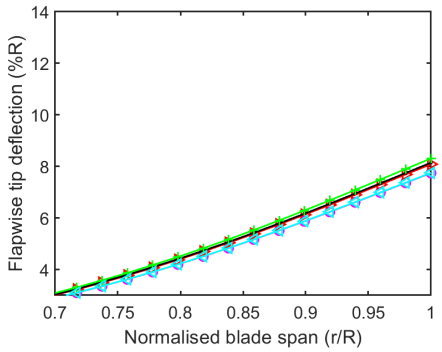

(c)

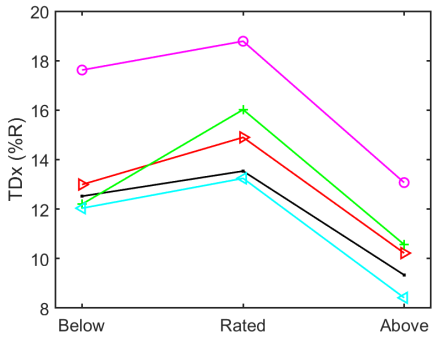

(d)

Figure 3: Normalised blade tip flapwise displacement: Time-averaged plots (a,b,c). a) Below rated ($V_{hub} = 8.5\,\mathrm{m/s}$) b) Around Rated ($V_{hub} = 11.5\,\mathrm{m/s}$) c) Above rated ($V_{hub} = 14.5\,\mathrm{m/s}$) d) Maximum values at tip, at different wind speeds

The trends in Figure 3 follow the same trend as that in normal force seen in Figure 2. A higher time-averaged flapwise deflection is noted in the SABL inflow, at and above rated wind speeds. A 1% higher normalised flapwise deflection represents roughly 1.5 m increase for the IEA 22 MW RWT. Once again, the maximum value is present for the IEC NTM scenario and the other scenarios are under that value. This is mainly because the rotor is exposed to higher wind speeds due to higher turbulence levels. Figure 4 provides more insight into the blade flapwise deflection at various azimuthal positions.

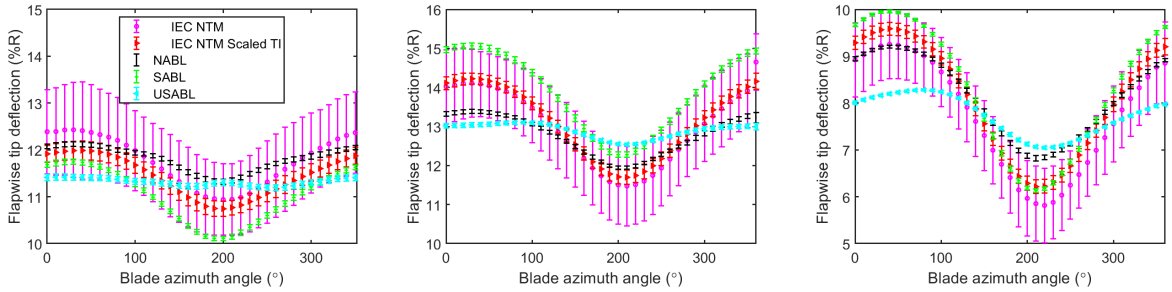

(a) (b) (c)

Figure 4: Bin averaged azimuthal variation of normalised blade tip flapwise displacement. Azimuth angle of 0 deg corresponds to the blade 1 in the up position, that is, opposite to gravity. The error bar represents the standard deviation. a) Below rated ($V_{hub} = 8.5\,\mathrm{m/s}$) b) Around Rated ($V_{hub} = 11.5\,\mathrm{m/s}$) c) Above rated ($V_{hub} = 14.5\,\mathrm{m/s}$)

In Figure 4, a first observation that can be made is that an almost consistently higher time-averaged flapwise deflection is seen for the SABL case, around and above rated wind speeds. It can also be noted that due to the elevated turbulence levels in the IEC NTM case, the time averaged flapwise tip deflection has variations of about 2% R or 3 m. Apart from the USABL case, the trough in the flapwise tip deflection is seen at roughly 200 deg which represents the position when the blade tip is exposed to a lower wind speed. The USABL case has a complex shear as evident in Figure 1, which leads to the deviation from the normal trend.

Figure 5 below illustrates the angle of attack at 50% span location, through the different azimuthal locations.

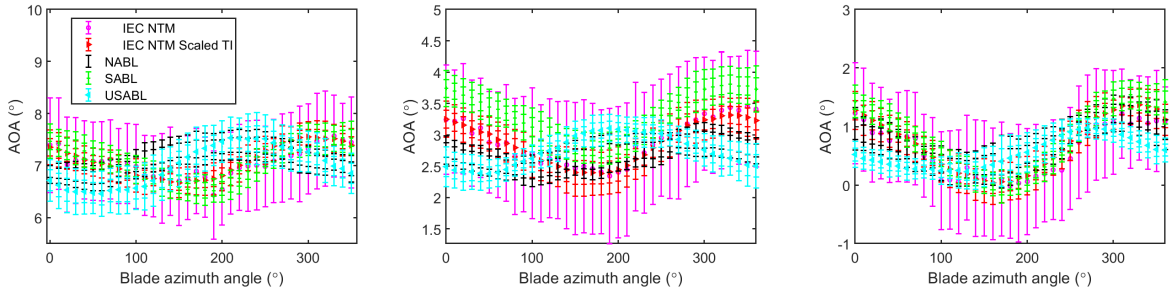

(a) (b) (c)

Figure 5: Bin averaged azimuthal variation of local angle of attack at 0.5 r/R. Azimuth angle of 0 deg corresponds to the blade 1 in the up position, that is, opposite to gravity. The error bar represents the standard deviation. a) Below rated ($V_{hub} = 8.5\,\mathrm{m/s}$) b) Around Rated ($V_{hub} = 11.5\,\mathrm{m/s}$) c) Above rated ($V_{hub} = 14.5\,\mathrm{m/s}$)

Once again, it can be noted that the USABL case has a different trend in the three wind speed regions, than the other cases. The differences in angle of attack are upto 3 deg for the IEC NTM case and about 1 deg for the other cases. At higher wind speeds, it is seen that the angle of attack is lower owing to the higher blade pitch. It should be noted that the absolute values of angle of attack may not be fully realistic because of no blade- torsion degree of freedom in the current study.

Finally, to assess the fatigue loads, a fatigue assessment based on the damage equivalent load formulation (corrected for mean stress) of [24] was used with the input of the blade root flapwise bending moment spectrum. The damage equivalent spectrum (S_{eq}) was found with the following equation:

$$S_{r,eq} = \left(\frac{\sum_{i=1}^{n} \left(S_{r,i} \frac{S_u - |S_{m,eq}|}{S_u - |S_{m,i}|} \right)^m}{N_{eq}} \right)^{\frac{1}{m}} \tag{2}$$

$S_{r,i}$ is the range (difference of maximum and minimum value) of the i^{th} load cycle and $S_{m,i}$ is the mean of the i^{th} load cycle. N_{eq} was chosen as $10e6$, roughly the number of 10 minute periods in a 20 year span and $S_{m,eq}$ as 0. Finally, to select S_u, the authors propose to evaluate it at different $\frac{S_{max}}{S_u}$ ratios. So, the value of S_{max} is used which corresponds to the maximum bending moment in the retrofitted case, different for each wind speed bin. The value of S_{max} which corresponds to the maximum bending moment for the respective wind speed was chosen and $\frac{S_u}{S_{max}} = 0.4$ along with a Wöhler exponent of $m = 10$.

Figure 6 provides the relative difference of the damage equivalent blade root flapwise bending moment, in comparison to the IEC NTM case.

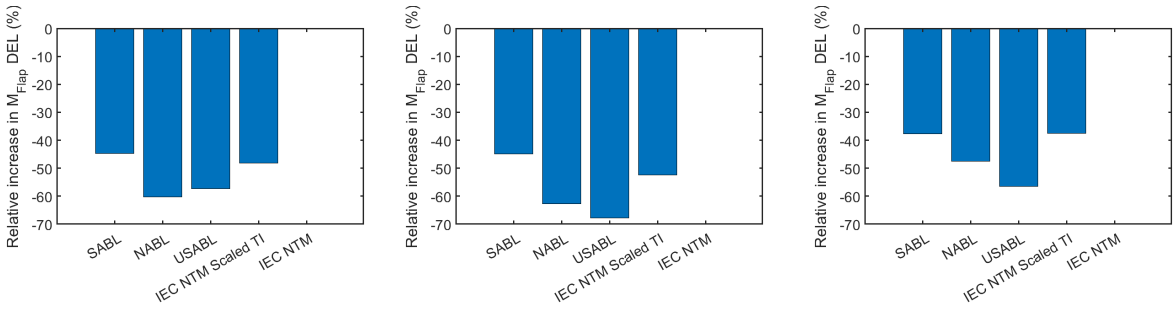

(a) (b) (c)

Figure 6: Damage equivalent blade root flapwise bending moment relative difference. a) Below rated ($V_{hub} = 8.5\,\mathrm{m/s}$) b) Around Rated ($V_{hub} = 11.5\,\mathrm{m/s}$) c) Above rated ($V_{hub} = 14.5\,\mathrm{m/s}$)

From Figure 6 it can be observed that the IEC NTM case has a significantly higher damage equivalent load. The main reason being the high turbulence level, as mentioned previously, being roughly 17% for the IEC NTM case while less than 5% for the higher fidelity inflows.

5. Conclusions

This study assessed the IEA 22 MW RWT in various inflow conditions. Lower and higher fidelity methods were used to generate 15 different inflow conditions. The former employed the IEC Kaimal turbulence model, while the latter employed Large Eddy Simulations. Standalone OpenFAST simulations were conducted using the NREL ROSCO controller in the respective inflow conditions. Regarding the inflow conditions, it was found that the wind shear is highest in a stable atmosphere compared to the power law wind profile of exponent 0.14 for offshore conditions specified by IEC standards, while lowest for unstable atmospheric conditions. A considerably lower hub height turbulence intensity, $\leq$ 5% was observed in the higher fidelity inflow wind fields, attributed to the lower surface roughness and a high hub height of 170 m. In regards to the rotor performance, it was found that the time-averaged design loads were higher, up to 7%, for the stable atmosphere, at and above rated wind speeds, while lower for below-rated wind speeds, in comparison to the IEC NTM case. However, the maximum design loads were higher for the IEC NTM case, as also observed in previous studies for smaller wind turbines ($\leq$ 10 MW). A considerably lower damage equivalent load, lower by 30% to 70%, was evident for the different scenarios, in comparison to the IEC NTM case.

The results show that the current IEC standards lead to a conservative design, but the statement cannot be made certain until more cases are analysed. Further studies will encompass more cases and involve small wind farm scenarios to establish typical levels of wake-added turbulence at such high hub heights. Furthermore, it could be worthwhile to investigate the rotor performance using higher fidelity models instead of BEM, and using nonlinear structural solvers to get further insights into the structural performance.

Acknowledgments

This research was supported by Korea Institute of Energy Technology Evaluation and Planning(KETEP) grant funded by the Korea Government (MOTIE) (20228520020050).

References

[1] Stull R 2017 *Practical Meteorology: An Algebra-based Survey of Atmospheric Science* ISBN 978-0-88865-283-6 URL https://www.eoas.ubc.ca/books/Practical_Meteorology/

[2] Wharton S and Lundquist J K 2012 *Environmental Research Letters* **7** 14005 URL https://dx.doi.org/10.1088/1748-9326/7/1/014005

[3] International Electrotechnical Commission (IEC) IEC 61400-3-1:2019 — IEC Webstore URL https://webstore.iec.ch/publication/29360
[4] IEA Wind Task 37 2023 IEAWindTask37/IEA-22-280-RWT URL https://github.com/IEAWindTask37/IEA-22-280-RWT
[5] Sartori L, Bellini F, Croce A and Bottasso C L 2018 *Journal of Physics: Conference Series* **1037** 042003 ISSN 1742-6596 URL https://iopscience.iop.org/article/10.1088/1742-6596/1037/4/042003
[6] Veers P, Bottasso C L, Manuel L, Naughton J, Pao L, Paquette J, Robertson A, Robinson M, Ananthan S, Barlas T, Bianchini A, Bredmose H, Horcas S G, Keller J, Madsen H A, Manwell J, Moriarty P, Nolet S and Rinker J 2023 *Wind Energy Science* **8** 1071–1131 ISSN 23667451
[7] Holtslag M C, Bierbooms W A and van Bussel G J 2016 *Wind Energy* **19** 1917–1932 ISSN 1099-1824 URL https://onlinelibrary.wiley.com/doi/full/10.1002/we.1959
[8] Hansen K S, Larsen G C and Ott S 2014 *Journal of Physics: Conference Series (Online)* **524** 012165 ISSN 1742-6596 URL https://orbit.dtu.dk/en/publications/dependence-of-offshore-wind-turbine-fatigue-loads-on-atmospheric-
[9] Lee S, Churchfield M, Moriarty P, Jonkman J and Michalakes J 2012 URL https://www.nrel.gov/docs/fy12osti/53567.pdf
[10] Ameya Sathe and Wim Bierbooms 2007 *Journal of Physics: Conference Series* **75** 012056 ISSN 1742-6596 URL https://dx.doi.org/10.1088/1742-6596/75/1/012056
[11] Schepers G, Van Dorp P, Verzijlbergh R, Baas P and Jonker H 2021 *Wind Energy Science* **6** 983–996 ISSN 23667451
[12] Zahle F, Barlas T, Lønbæk K, Bortolotti P, Zalkind D, Wang L, Labuschagne C, Sethuraman L and Barter G 2024 Definition of the IEA Wind 22-Megawatt Offshore Reference Wind Turbine Tech. rep. DTU Wind and Energy Systems
[13] Jonkman B J 2014 TurbSim User's Guide Tech. rep. National Renewable Energy Laboratory (NREL) URL www.nrel.gov/publications.
[14] NREL 2022 SOWFA: Simulator fOr Wind Farm Applications URL https://www.nrel.gov/wind/nwtc/sowfa.html
[15] Weller H G, Tabor G, Jasak H and Fureby C 1998 *Computer in Physics* **12** 620–631 ISSN 0894-1866 URL /aip/cip/article/12/6/620/510187/A-tensorial-approach-to-computational-continuum
[16] Churchfield M, Lee S and Moriarty P 2012 Overview of the Simulator fOr Wind Farm Application (SOWFA) Tech. rep. National Renewable Energy Laboratory (NREL), U.S.A URL https://www.nrel.gov/wind/nwtc/assets/pdfs/sowfa-tutorial.pdf
[17] Gebraad P M O, Churchfield M J and Fleming P A 2016 *Journal of Physics: Conference Series* **753** 52004 URL https://dx.doi.org/10.1088/1742-6596/753/5/052004
[18] Jonkman J, Sprague M and et al 2022 OpenFAST — Wind Research — NREL URL https://www.nrel.gov/wind/nwtc/openfast.html
[19] Quon E, Churchfield M, Cheung L and Kern S 2017 Development of a Wind Plant Large-Eddy Simulation with Measurement-Driven Atmospheric Inflow *American Institute of Aeronautics and Astronautics SciTec* (Grapevine, Texas) URL http:/www.osti.gov/scitech
[20] Gadde S N and Stevens R J 2021 *Journal of Renewable and Sustainable Energy* **13** 13305 ISSN 19417012 URL /aip/jrse/article/13/1/013305/284849/Effect-of-low-level-jet-height-on-wind-farm
[21] Delft High Performance Computing Centre (DHPC) 2022 DelftBlue Supercomputer (Phase 1) https://www.tudelft.nl/dhpc/ark:/44463/DelftBluePhase1
[22] NREL 2021 ROSCO. Version 2.4.1 URL https://github.com/NREL/ROSCO
[23] The Mathworks I MATLAB:R2021a URL https://nl.mathworks.com/products/matlab.html
[24] Hendriks H B and Bulder B H 1995 Fatigue Equivalent Load Cycle Method Tech. rep. Energy Research Centre of the Netherlands (ECN) Petten URL https://publicaties.ecn.nl/PdfFetch.aspx?nr=ECN-C--95-074